ORCA – Online Research @ Cardiff

Monitoring Water Clarity Using Landsat 8 Imagery in Jiaozhou Bay, China, From 2013 to 2022

Dingfeng Yu, *Member, IEEE*, Tengda Qi, Lei Yang, Yan Zhou, Chunyan Zhao, and Shunqi Pan

Abstract—Secchi disk depth (SDD) is a crucial indicator for assessing changes in the water environment. Coastal water transparency varies due to weather, climate, and human activities. Systematic observations are crucial for assessing water quality and ecosystem health. This study used Landsat 8 imagery to investigate the transparency of Jiaozhou Bay (JZB) from 2013 to 2022 and to explore the primary factors influencing transparency changes. Among natural factors, precipitation plays a dominant role in transparency changes. After 2019, there was an increase in rainfall in JZB, which usually leads to reduced transparency. However, the significant improvement in transparency, attributed to a sharp reduction in human activities due to the coronavirus disease 2019, highlights the substantial impact of human activities on JZBs transparency.

Index Terms—Jiaozhou Bay (JZB), Landsat, offshore waters, remote sensing, Secchi disk depth (SDD).

I. INTRODUCTION

COASTAL waters are vital ecosystems for marine life. They play a crucial role in safeguarding marine biodiversity and stability, facilitating transportation and human mobility,

Dingfeng Yu, Lei Yang, and Yan Zhou are with the Institute of Oceanographic Instrumentation, Qilu University of Technology (Shandong Academy of Sciences), Qingdao 266100, China, also with the National Engineering and Technological Research Center of Marine Monitoring Equipment, Qilu University of Technology (Shandong Academy of Sciences), Qingdao 266100, China, and also with the Shandong Provincial Key Laboratory of Marine Monitoring Instrument Equipment Technology, Qilu University of Technology (Shandong Academy of Sciences), Qingdao 266100, China (e-mail: dfyu@qlu.edu.cn; yangleibest@qlu.edu.cn; zhouyan_ocrs@qlu.edu.cn).

Tengda Qi and Chunyan Zhao are with the Institute of Oceanographic Instrumentation, Qilu University of Technology (Shandong Academy of Sciences), Qingdao 266100, China (e-mail: qtd6598729@hotmail.com; chunyanzhao2021@163.com).

Shunqi Pan is with the Hydro-Environmental Research Centre, School of Engineering, Cardiff University, CF24 3AA Cardiff, U.K. (e-mail: pans2@cardiff.ac.uk).

and supporting regional economic development. However, over the past few decades, economic development in coastal cities has placed significant pressure on the water quality of coastal areas due to human activities, such as industrial operations and large-scale discharge of urban sewage. Within this ecosystem, hazardous algal blooms and other dangerous events have become increasingly frequent, leading to a decline in both the variety and population of marine species. This has had a profound impact on the local coastal communities, resulting in economic losses and ecological disruption. Therefore, thorough, accurate, and continuous monitoring of such water bodies is of paramount importance [1].

Transparency is a crucial parameter for assessing water quality, eutrophication level, and describing the optical properties of water bodies [2]. It is also closely related to environmental parameters, such as chlorophyll-a concentration, total suspended solids concentration, colored dissolved organic matter concentration, sea surface salinity, and sea surface temperature. Therefore, transparency is a commonly used indicator for the assessment of marine environmental quality [3], [4].

The traditional method for measuring transparency is the Secchi disk method. However, this method is limited by the measurement range and time costs, which often results in discrete and sparse measurement data. In contrast, remote sensing techniques can rapidly and effectively cover large areas to measure the water transparency. This overcomes the limitations of traditional measurement methods and has become one of the important research tools for monitoring water transparency [5], [6]. In recent years, there has been an increasing trend of applying remote sensing methods to study water transparency. For instance, Suffian et al. [7] utilized moderate-resolution imaging spectroradiometer (MODIS) satellite data to retrieve water clarity on the Eastern coast of the Malaysian Peninsula and the Malacca Strait and analyzed the seasonal and interannual variations in water clarity within this region. Daniel et al. [8] developed a semianalytical algorithm based on moderate-resolution medium-resolution imaging spectrometer (MERIS) satellite data and assessed its performance by utilizing MERIS images obtained over Kasumigaura Lake in Japan. Yousef et al. [9] utilized sea-viewing wide field-of-view sensor (SeaWiFS) and MODIS data to assess water clarity in Lake Superior, Lake Michigan, and Lake Huron, and analyzed the interannual variations in water clarity from 1998 to 2012. Zhou et al. [10] conducted a remote sensing retrieval of water clarity in JZB based on geostationary ocean color imager (GOCI) data and investigated its diurnal variations. Zhang and Zeng [11] established a remote sensing retrieval model for water

clarity in the Taiwan Strait using MODIS satellite data, analyzing the distribution patterns and variability in water clarity. JZB is relatively compact in size, but satellites with low spatial resolution, such as MODIS, MERIS, SeaWiFS, and GOCI, are incapable of detecting minor variations in water transparency so that this study is to use the Landsat 8 satellite data with a spatial resolution of 30 m to examine spatiotemporal fluctuations in water transparency and their contributing factors in the JZB area, which is located in the western coast of Bohai Sea.

In general, remote sensing inversion of water transparency used in these studies adopts the empirical methods [12]. However, the empirical methods are only applicable to water bodies with similar optical variable compositions because the algorithm coefficients depend on the dataset used during algorithm development. To overcome the limitations of empirically derived Secchi disk depth (SDD) inversion, a mechanism algorithm based on ocean color measurements has been developed. Lee et al. [13] re-evaluated the classical theoretical explanation of SDD and introduced a novel underwater visibility model, which was validated through field measurements in bays, lakes, and other water body types, demonstrating a strong alignment between the in situ SDD and the derived SDD. Subsequently, Lee et al. [14] parameterized the SDD model using Landsat 8 imagery and applied it to the Jiulong River in Fujian Province, China. The resulting spatial distribution of SDD derived from the field measurements agreed well with the visual observations. Therefore, further to the work of Lee et al. [13], a semianalytical algorithm is developed to extract water transparency data from Landsat 8 remote sensing imagery of JZB in the period from 2013 to 2022.

II. MATERIALS AND DATA

A. Study Area

Jiaozhou Bay is located on the southern side of the Shandong Peninsula, with coordinates between 35°38′N to 36°18′N latitude and 120°04′E to 120°23′E longitude. It is a semienclosed, fan-shaped bay bordered by Tuandaotou (36°02′36″N, 120°16′49″E) and Xuejiadao Jiaozishi (36°00′53″N, 120°17′30″E) [15]. JZB covers an area of approximately 390 km², with an average depth ranging from 6 to 7 m. Most areas within the bay have depths of less than 5 m [16]. The vicinity of JZB hosts a diverse wetland ecosystem comprising mangroves, grasslands, and marshes, offering ample habitats for a variety of flora and fauna. In addition, the bay shelters a wide array of marine biodiversity, encompassing diverse fish, crustaceans, and avian species. As depicted in Fig. 1(a), the aquatic environment in JZB is affected by inflowing rivers from the mainland, such as the Licun River, Yang River, Dagu River, and among others. Meanwhile, human activities in the vicinity, including industrial emissions, urban sewage, and overfishing, have exerted a discernible impact on the ecological equilibrium of the Bay region. To safeguard and preserve the ecological integrity of JZB, pertinent authorities have instituted a range of measures, encompassing wetland conservation, water management, and ecological restoration, with the aim of ensuring the sustainable development of the
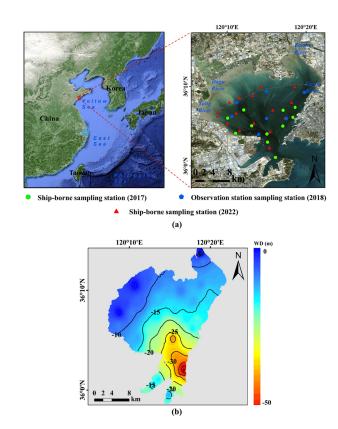

Fig. 1. (a) Locations of JZB and the sampling stations. (b) Water depth in JZB.

bay region. The construction of the JZB cross-sea bridge, which commenced in 2007, also altered the original hydrodynamic environment to some extent. JZB, a typical coastal ecosystem in China, stands out as an excellent research area for monitoring coastal ecosystem health. Conducting comprehensive research on the transparency of JZB plays a crucial role in understanding and assessing the environmental health and ecological dynamics of the region. A thorough understanding of JZBs transparency not only reveals the potential impacts of human activities on the region's ecological balance but also forms a scientific basis for developing comprehensive conservation plans. By guiding the implementation of measures, such as ecological restoration, water quality management, and wetland conservation in the bay area, we can better ensure the sustainable development of JZBs aquatic resources and promote the long-term ecological health of the region. Therefore, a comprehensive understanding of water clarity holds undeniable scientific value for maintaining the ecological balance of JZB and promoting its long-term health. Moreover, the distribution characteristics of water clarity in JZB offer valuable insights for marine resource management, port development, navigation, aquaculture, environmental protection, and regional development planning [17].

B. In Situ Data

The in situ SDD data for JZB used in this study were primarily sourced from shipborne field scientific experiments and fixed observation stations, as depicted in Fig. 1(a). Shipborne field scientific experiments were conducted on clear days during

TABLE I
DETAILS OF SDD MEASURED IN JZB

Measurement method	Date	Measurement stations
Ship-borne sample	2017.05.16	11
	2022.10.28	9
	2022.11.01	9
Observation station sample	2018.03.09	6
	2018.03.12	5
	2018.06.13	7
	2018.06.20	4
	2018.09.12	8
	2018.09.13	3
	2018.12.12	6
	2018.12.13	2
	2018.12.14	3

TABLE II
LIST OF LANDSAT 8 IMAGES ANALYZED

Year	Quantity of images
2013	6
2014	13
2015	6
2016	8
2017	12
2018	11
2019	10
2020	7
2021	8
2022	10

three voyages: May 16, 2017, October 28, 2022, and November 1, 2022. The Secchi disk method was employed for in situ transparency measurements. In situ SDD data from fixed observation stations were obtained from the Shandong JZB Marine Ecosystem National Field Scientific Observation and Research Station.[1] Eight fixed observation stations contributed to a total of 44 measured transparency data points. Most of the transparency measurements were conducted in March, June, September, and December of 2018. Table I presents the temporal distribution of in situ SDD data.

C. Satellite Data

The Landsat 8 satellite operates on a revisit period of 16 days. The temporal misalignment between effective satellite image acquisition and in situ data sampling is a notable concern. Nonetheless, He et al. [18] assert that employing in situ data collected within a seven-day window around the time of satellite image acquisition is a viable practice. Olmanson et al. [19] contend that the increase in the time gap between field data sampling and satellite imagery has a minimal impact on the correlation between the inversion results and in situ data. Consequently, to ensure both the effectiveness and accuracy of the algorithm model, we opted for a dataset with seven days interval for assessing its performance. Considering the field data collection dates, as listed in Table I, alongside the acquisition times of Landsat 8 satellite images, it was determined that 33 observation stations met the criteria on May 16, 2017, March 9, 2018, June 13, 2018, and October 28, 2022. After excluding observation points beyond the study area, 22 datasets were chosen for the analysis of the algorithm's performance.

The Landsat satellite series has consistently monitored Earth for over half a century, capturing millions of invaluable images with the instruments onboard. These resources are instrumental for global change research and find applications in diverse fields, such as agriculture, cartography, forestry, regional planning,

surveillance, and education [20]. The Landsat 8 data used in this study were sourced from the official USGS website (http://www.usgs.gov/), with all images encompassing the JZB from 2013 to 2022 being downloaded. Images with a cloud cover exceeding 80% were excluded, leaving 91 images for subsequent spatiotemporal change analysis (see Table II). The primary preprocessing steps for Landsat data include radiometric calibration and atmospheric correction. In this study, atmospheric correction was executed using the fast line-of-sight atmospheric analysis of the spectral hypercubes radiative transfer model, which is based on MODTRAN5.

D. Meteorological and Hydrological Data

Meteorological and hydrological data for this study were obtained from the Jiaozhou Bay National Marine Ecosystem Research Station[2], including monthly precipitation, average 10-min wind speed, and air temperature. Runoff data, covering the annual average rainfall from 2013 to 2022 for the Nancun Hydrological Station in the Dagu River, were acquired from the Qingdao Hydrological Bureau.[3] Water depth data were extracted from 15 arc-sec resolution DEM data (ETOP 2022) provided by the U.S. National Center for Environmental Information[4], which offered the bathymetry of JZB and the water depth in JZB is shown in Fig. 1(b).

III. METHODOLOGY

A. SDD Inversion Algorithm

In 2015, Lee et al. [13] refined the classical underwater visibility theory and introduced a novel theoretical model for inversely estimating transparency. This model solely relies on the minimum diffuse attenuation coefficient (K_d) within the visible light wavelength range and has been validated using datasets from bays, lakes, and other aquatic environments. The results exhibit a close correlation with field-measured data, with a determination coefficient (R^2) of 0.96. The model is expressed

as follows:

$$Z_{\mathrm{SD}} = \frac{1}{2.5\mathrm{Min}(K_d^{tr})} \ln\left(\frac{|0.14 - \mathrm{R}_{\mathrm{rs}}^{tr}|}{0.013}\right). \qquad (1)$$

In (1), K_d^{tr} represents the minimum diffuse attenuation coefficient of the water within the visible light spectrum (400–700 nm), and R_{rs}^{tr} denotes the corresponding remote sensing reflectance in this wavelength range. The formula yields an R^2 value of 0.803, a mean relative error of 13.2%, and a root-mean-square error of 0.209 m. The Landsat 8 satellite utilizes wavelengths at 443, 481, 554, and 656 nm. Lee et al. estimated the diffuse attenuation coefficient at 530 nm using an empirical algorithm to bridge the broad spectral gap between 481 and 554 nm.

B. Trend Analysis

This study employed the Mann–Kendall (MK) and Sen's slope (Sen) methods to assess the spatial distribution and temporal changes in transparency. These methods are commonly used in long-term time-series analysis in hydrometeorological studies. MK, a nonparametric statistical test, is well suited for analyzing trends in hydrological characteristics. Sen, on the other hand, is a statistical method used to estimate trends in datasets. It can mitigate the impact of data deletion and outliers on statistical results by constructing order sequences based on varying sample lengths, thus enabling the identification of trends and degrees of change in time series. Sen and MK were leveraged in this study to examine annual variations in transparency, providing corresponding transparency trend analysis results for the respective time periods.

C. Empirical Orthogonal Function (EOF) Decomposition

Lorenz introduced the EOF to meteorological and climatic research, which has since found extensive applications in various disciplines, including geoscience and environmental science [21], [22].

In this study, the covariance matrix method was used to conduct EOF decomposition on monthly mean SDD from JZB. To address the challenge posed by an abundance of pixel data in Landsat 8 images of JZB, a spatiotemporal transformation technique was implemented. This technique prevented an undue escalation of the covariance matrix order. Finally, the North test was utilized to evaluate the physical meaningfulness of the EOF analysis outcomes.

IV. RESULTS

A. Validation

After preprocessing Landsat 8 imagery, the Lee_2015 model [14] was used to estimate SDD values. As shown in Table III, the statistics and comparison of in situ data and inversion data were conducted. Statistical analysis (p-value < 0.01, $R^2 = 0.78$) in Fig. 2 revealed a significant correlation between the estimated SDD values and the measured data. The inversion results obtained with the Lee_2015 model for Landsat 8 were linearly corrected using the measured data, yielding a slope of 0.715,

TABLE III
COMPARISON OF STATISTICAL INFORMATION BETWEEN IN SITU DATA AND INVERSION DATA

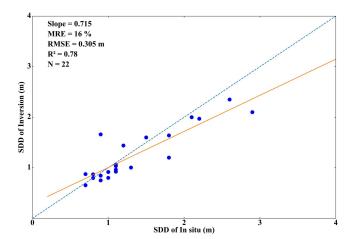|	Quantities	Min (m)	Average (m)	Max (m)	Variance (m²)
In situ data	73	0.6	2.006	5.8	1.118
Inversion data	22	0.653	1.248	2.35	0.257

Fig. 2. Contrast results between the measured values and in situ values for SDD.
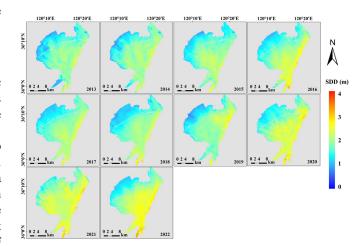
Fig. 3. Annual mean SDD distribution from 2013 to 2022.

intercept of 0.29, and RMSE of 0.305 m. These results demonstrate the model's high precision, making it suitable for SDD retrieval in the study area.

B. SDD Interannual Distribution

Fig. 3 shows a trend of higher transparency in the southeast JZB and lower transparency in the northwest JZB. This trend corresponds with the depth distribution of the water [see Fig. 1(b)], which gradually increases from the northwest to the southeast and southern parts. The transparency in JZB is directly

Fig. 4.   Annual mean SDD changes from 2013 to 2022.

Fig. 5.   Change of SDD from 2013 to 2022. (a) Sen. (b) MKZ.

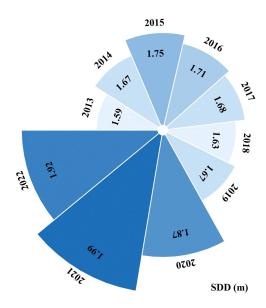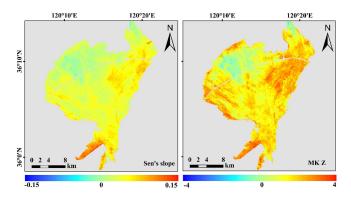proportional to water depth. In the northwest part of JZB, the seawater is relatively shallow and influenced significantly by rivers, such as Dagu River and Yang River, as well as tides, resulting in lower transparency. Using the JZB bridge as a dividing line, the transparency in the northern area generally does not exceed 2 m, while in the southern area, it is often greater than 2 m. This spatial distribution is consistent with the findings of Yin et al. [23].

Fig. 4 displays the trend in annual mean SDD in JZB from 2013 to 2022. Over the course of ten years, there is a clear upward trend in SDD, with annual mean values ranging from 1.59 to 1.99 m. In 2013, the annual mean SDD was the lowest at 1.59 m, and in 2021, it reached the highest at 1.99 m. The years 2019 and 2020 are clearly seen the largest variation in annual mean SDD, with an increase of 0.2 m.

C. Interannual Trends in SDD

To assess the spatiotemporal trends in SDD in JZB, Sen's slope was employed to calculate the slope of the data series, representing the degree of variation in transparency values over time. Simultaneously, the MK test was used to assess temporal changes and the significance of the trend. Fig. 5 presents the
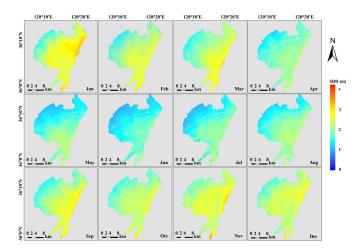

Fig. 6.   Monthly mean SDD distribution from 2013 to 2022.

analysis of Sen's slope estimates for SDD in JZB from 2013 to 2022, along with MK test results. The results indicate that, except for areas near Dagu River and Baisha River, which show a decreasing trend, changes are not significant. Some areas along the northwest coast exhibit a slight increasing trend, possibly due to tidal influences. In other regions, there has been a mild upward trend over the past decade. Notably, the most pronounced increase in transparency is observed in the southwest area (Qingdao Qianwan Bonded Port Zone). This could be attributed to the establishment of the Qingdao Qianwan Bonded Port Zone, approved by the State Council on September 7, 2008. In early 2013, the Qingdao Municipal Party Committee and Municipal Government expanded the planned development area of the Bonded Port Zone to 65.73 km^2. Initially, extensive shoreline reclamation during construction led to changes in sea area, sedimentation, and siltation. However, as construction was completed, there was a noticeable improvement in transparency in the corresponding area.

D. SDD Intermonth Distribution

Statistical analysis of multiyear monthly mean SDD changes, as shown in Figs. 6 and 7, indicates that the lowest monthly mean SDD occurs in June at 1.39 m, while the highest is observed in September at 2.3 m, while in September, it peaks at 2.3 m. Transparency consistently exhibits higher values in the southeast and lower values in the northwest, irrespective of the month. The transparency of JZB exhibits significant seasonal variations. Fig. 8 depicts the seasonal mean variations in SDD in JZB from 2013 to 2022. SDD reaches its lowest point during summer, with an average of only 1.49 m. In spring, there is a significant increase in water transparency, reaching a mean of 1.88 m. Winter exhibits the highest water transparency among all seasons, with an average of 2.2 m, while autumn's water transparency averages 1.9 m, generally lower than that of winter.

E. EOF Analysis of Intermonth Changes in SDD

Table IV presents the contribution rates of the first two characteristic vectors obtained from EOF decomposition and their
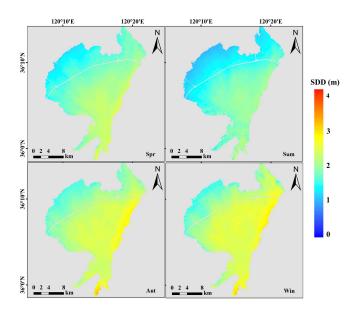
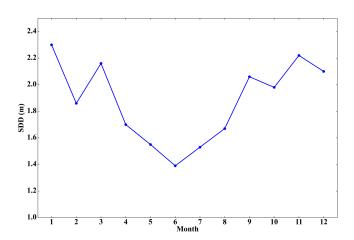Fig. 7. Seasonal mean SDD distribution from 2013 to 2022.

Fig. 8. Monthly mean SDD changes from 2013 to 2022.

TABLE IV
COEFFICIENT OF TIME AND ITS CORRELATION WITH INFLUENCING FACTORS

	Variance contribution rate	Precipitation	Temperature	Wind speed
EOF1	0.720	-0.653	-0.528	-0.413
EOF2	0.101	0.233	-0.125	0.319

correlation coefficients with natural factors. Principal modes are derived through EOF decomposition, and further analysis is conducted on the spatial distribution, time-series amplitude, and major influencing factors of each principal mode. Each mode reflects variations in the original variable field, and the importance of a mode is determined by the size of its eigenvalue. The larger the eigenvalue, the more important the corresponding mode, indicating a higher contribution to total variance. The spatial distribution and temporal amplitude of each mode jointly
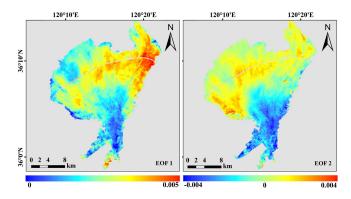

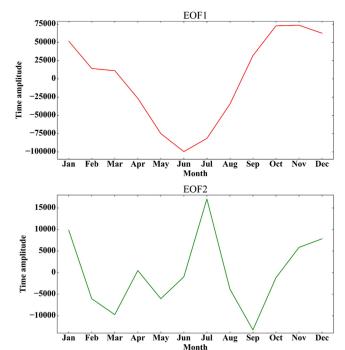Fig. 9. Spatial distribution of EOF modes.

Fig. 10. Interannual changes of EOF modes.

determine the increase or decrease in pixel values. One influencing factor can appear in several major modes, and one mode may be related to multiple factors.

Fig. 9 displays the spatial distribution of the first two modes obtained from EOF decomposition, while Fig. 10 displays their corresponding time-series amplitude plots. The first mode, contributing 72.01% of the total variance, significantly influences overall transparency changes in JZB. Most regions exhibit positive spatial coefficients, indicating consistent transparency changes across JZB. The spatial coefficients gradually increase from the coastal areas to the JZB bridge area and then decrease toward the bay's mouth region. Except for the entrance area of the Dagu River, the JZB bridge area exhibits the greatest variation, indicating the highest variability in transparency values in this region, while other regions show relatively less change. The corresponding time amplitudes exhibit distinct seasonal cyclic characteristics: amplitudes are negative from April to August, suggesting that during this period, transparency in most areas is lower than the monthly average. Conversely, for other months,

time amplitudes are positive, indicating higher transparency than the monthly average. Given that water's optical components and temperature show seasonal cyclic characteristics, it can be inferred that they strongly correlate with this mode.

The second mode accounts for 10.14% of the total variance. Spatially, the northern part of JZB exhibits positive spatial coefficients, while the southern part shows negative coefficients, indicating a north–south difference in transparency. When transparency increases in the north, it decreases in the south, and vice-versa. Temporally, the coefficients show significant seasonal variations, with positive amplitudes in summer and winter, and negative amplitudes in spring and autumn. This suggests that transparency values increase in summer and winter, while they decrease in spring and autumn. Summer contributes most to this spatial pattern, with other seasons contributing less. The seasonal amplitude differences may be due to the influence of runoff and wind speed in the northern part of JZB, leading to suspended sediment. In contrast, in the southern part, water mass exchange at the mouth of JZB and the construction of the JZB bridge significantly impact areas near the bridge's north and south sides. However, most areas in the southern part of JZB are less affected, resulting in north–south differences [24].

V. DISCUSSION

A. Natural Factors

The Dagu River, one of the major rivers flowing into JZB, boasts the largest basin coverage, making up 82% of the total basin area of all rivers entering the bay [25]. Its primary water source is precipitation, making it a typical rainfall-fed river. Research indicates a negative correlation between SDD and the river water's flow and velocity. This correlation primarily stems from the fact that a greater flow enhances the erosive capabilities of the water flow, leading to increased sediment transportation and higher suspended particle content within the basin, thereby reducing transparency [26]. The runoff data utilized in this study comprise monthly data from the Nancun Hydrological Station spanning from 2013 to 2022. The distribution of annual water discharge in the Dagu River's main stream is notably uneven throughout the year. Water discharge at the Nancun Hydrological Station is predominantly concentrated during the flood season (June to September), accounting for approximately 94.8% of the annual water discharge. In contrast, water discharge from October to December is relatively minimal, making up about 3.2% of the annual water discharge; from January to May, it is at its lowest, accounting for approximately 2.0% of the annual water discharge. As can be inferred from Fig. 11, there exists a negative correlation between precipitation and transparency.

From 2013 to 2022, transparency data for JZB, along with monthly precipitation, wind speed, and temperature data, were monthly averaged and subjected to comparative analysis for each of the 12 months. As depicted in Fig. 12, JZB experiences the highest rainfall and temperature during the summer season. This leads to increased runoff from inflowing rivers, such as Dagu River, Baisha River, Yang River, and Licun River, which carry sediment into JZB. This leads to increased suspended particles
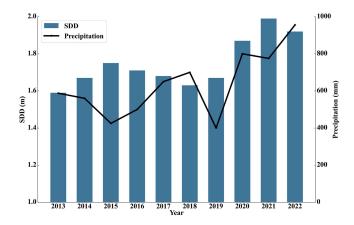

Fig. 11. Correlation between the annual mean SDD in JZB and the annual mean precipitation values at the Nancun hydrological station from 2013 to 2022.
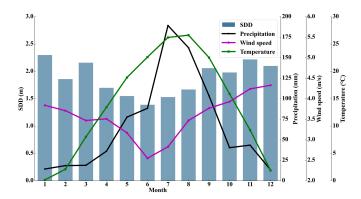

Fig. 12. Correlation between the monthly mean SDD and the monthly mean values of precipitation, wind speed, and temperature in JZB from 2013 to 2022.

in the water and a subsequent decrease in transparency. Stronger winds lead to a higher concentration of suspended sediment in the water, particularly in shallow areas, resulting in reduced transparency.

To identify the primary environmental factors influencing monthly SDD variation, Table IV displays correlation coefficients between the time coefficients in the first and second modes and environmental factors. The first mode shows a significant negative correlation with wind speed, precipitation, and temperature. The highest correlation coefficient is observed with precipitation ($r = -0.653$), while temperature ($r = -0.528$) and wind speed ($r = -0.413$) show relatively smaller correlation coefficients. This suggests that SDD is primarily influenced by precipitation, while temperature and wind speed act as covariates. The time coefficient in the second mode shows the highest correlation with wind speed, albeit weaker.

Vegetation plays a crucial role in the conservation of water resources, maintenance of soil integrity, reduction of river sediment content, and moderation of runoff variability. These factors indirectly influence the SDD in JZB. This study utilizes the kernel normalized difference vegetation index to estimate fractional vegetation cover (FVC) within the JZB basin [27]. FVC distribution within JZB was analyzed based on the classification of FVC [28], revealing a low level of vegetation coverage in the
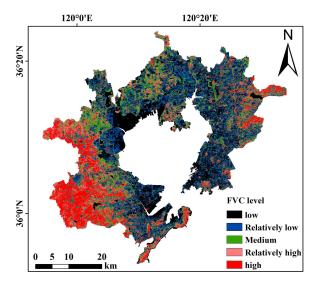
Fig. 13.   Distribution of FVC in the areas adjacent to JZB in 2019.

Fig. 14.   (a) Medical waste in JZB. (b) Enteromorpha in JZB. (c) Oil spill from a cargo ship in JZB.

JZB basin. Fig. 13 shows the distribution of FVC in the areas adjacent to JZB in 2019. To eliminate the impact of COVID-19 on SDD, we conducted an analysis comparing the annual average vegetation coverage percentage in the JZB basin from 2013 to 2019. The highest correlation ($r = -0.94$ and $p = 0.0012$) was observed between SDD and the sum of low and relatively low vegetation coverage.

B. Human Factors

Human activities in JZB primarily consist of aquaculture, marine transportation, port facility construction, and coastal development. The COVID-19 imposed restrictions on many human activities, providing the ocean with a period of respite. It has had a significant impact on not only maritime industries, tourism, and fisheries but also the marine ecological environment. Some of these impacts have been positive. Research indicates that during the initial outbreak of the pandemic, the reduction in shipping and fisheries activities, as well as the decline in coastal tourism, improved the marine ecological environment to some extent. Human activities along the coast of JZB and within the bay itself have also decreased sharply, directly affecting its ecological environment. While the reduction in human activities has greatly enhanced the marine ecological environment, there are also some harmful and irreversible impacts.

Fig. 14(a) illustrates that the COVID-19 has led to the usage of billions of masks worldwide each year, a substantial amount of plastic pollutants are discharged into the ocean, inflicting damage on the marine environment, particularly coastal ecosystems [29]. Statistics reveal that Asia and Europe collectively use approximately 350 billion masks annually, resulting in over 25 000 tons of plastic waste, including medical waste and personal protective equipment, being discharged into the ocean. This has emerged as a significant source of microplastic pollution. These pollutants, along with potential pharmaceutical residues, pose a considerable threat to nearshore ecosystems [30]. Fig. 11 shows that the annual mean transparency in JZB experienced its most
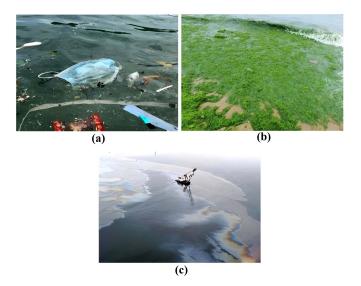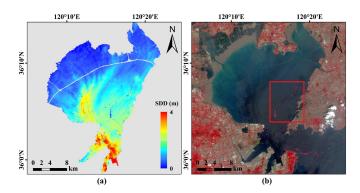

Fig. 15.   (a) SDD distribution of JZB on July 2, 2016. (b) False-color satellite image of JZB on July 2, 2016.

significant increase from 2019 to 2020. However, over time, the rate of transparency growth decreased, and by 2022, the annual mean transparency in JZB began to exhibit a declining trend. This trend could be attributed to the gradual stabilization of the pandemic, leading to regional policy changes that resulted in increased human activities. In addition, in 2022, the annual rainfall was relatively high compared to previous years, and another contributing factor could be the discharge of medical waste. The combined effects of these factors have significantly affected SDD.

COVID-19 caused the overall changes in the transparency of Jiaozhou Bay, while the outbreak of enteromorpha prolifera and ship transportation led to local changes in transparency. The outbreak of enteromorpha prolifera along the coast of northern Jiangsu drifted to JZB under the influence of the southeast monsoon and the current from south to north, leading to the outbreak of enteromorpha prolifera in JZB in summer [see Fig. 14(b)], and the SDD decreased linearly and areally in a short period [31]. Fig. 15 presents a false-color remote sensing image alongside the results of transparency inversion for JZB on July 2, 2016. It is apparent that the presence of drifting algae has led to a

Fig. 16. Qingdao municipal government policy timeline from 2013 to 2022.

systematic and localized reduction in transparency. Fig. 14(c) shows that pollutants, such as ship fuel, were emitted during ship navigation, raising suspended substances, such as sediments in the water, thereby affecting changes in SDD [32]. Ships in JZB mainly include fishing boats and cargo ships. However, the cargo throughput of Qingdao Port was minimally affected by COVID-19 and showed a growing trend year-by-year. Therefore, marine transportation had a small impact on the annual mean transparency change in JZB.

Moreover, the Qingdao Municipal Government has managed JZB through the implementation of various policies. As depicted in Fig. 16, the "Comprehensive Treatment Plan for the Pollution in the JZB Basin for 2013–2015," formulated by the Qingdao Municipal Government in 2013 and the "JZB Protection Control Line of Qingdao" approved by the 15th People's Congress Standing Committee of Qingdao have contributed to improving JZBs SDD. The enforcement of the "Regulations on the Protection of JZB of Qingdao" in 2014 and the "Notice on the Cleaning and Rectification of Fisheries and Aquaculture Facilities in JZB Sea Area" in 2015 further enhanced this transparency. However, with the 40th anniversary of reform and opening-up in 2016, and following the State Council's approval of the "Overall Urban Planning of Qingdao," improvements in urban infrastructure, development of marine economy and emerging industries, and construction of the West Coast New Area have somewhat reduced JZBs transparency. In 2018, comprehensive treatment projects for rivers, such as Licun River, Yang River, and Yuejin River, were initiated by the Qingdao Municipal Government, leading to an improvement in transparency. In June 2019, the "Work Plan for Winning the Battle of Pollution Prevention and Control in JZB and Its Coastal Waters" was issued by the Qingdao Municipal Government. Coupled with the outbreak of the COVID-19 at the end of 2019, there was a significant improvement in transparency. From 2020 onward, epidemic prevention and control became a top priority for the government while strictly enforcing the "Regulations on the Protection of JZB of Qingdao," effectively strengthening JZBs protection and restoration along with its inflowing rivers.

VI. Conclusion

Landsat 8 imagery from 2013 to 2022 was utilized to examine the spatiotemporal distribution characteristics of SDD in JZB over the past decade. The transparency dynamics within the study area were investigated using the Sen, MK, and EOF methods, and the impact of FVC and policies in the JZB basin on transparency was explored for the first time.

The quasi-analysis algorithm was utilized to achieve Landsat 8 satellite remote sensing monitoring of the SDD in JZB. The results indicated that the remotely sensed SDD is in good agreement with the measured SDD, with an MRE of 16% and an RMSE of 0.305 m. The spectral band configuration of the Landsat 8 satellite allowed for a relatively accurate estimation of JZBs transparency.

The spatial distribution pattern of transparency in JZB showed a characteristic of higher transparency in the southeast and lower transparency in the northwest. The distribution of transparency in the shallower waters of the western and northern areas formed a textured pattern influenced by tides. Overall, the distribution trend remained stable. Simultaneously, with the completion of the JZB bridge, there was a significant impact on water exchange in the northern part of the bay, leading to north–south differences in transparency.

The temporal distribution pattern of transparency in JZB exhibited fluctuations between 2013 and 2019, with minimal changes. Transparency showed an initial increase followed by a decrease from 2019 to 2022. In 2013, the mean transparency was at its lowest at 1.59 m, while in 2021, it reached its highest at 1.99 m. The period from 2019 to 2021 saw the greatest annual variation in transparency, with an increase of 0.32 m. Seasonal changes in transparency showed a pattern of initial decrease, followed by an increase, with summer having the lowest values, spring higher than summer, winter being the highest, and autumn following.

Natural factors, such as temperature, precipitation, and wind speed, significantly influenced the monthly variation in transparency in JZB, exhibiting a notable negative correlation. The combined effect of low and relatively low vegetation coverage has the greatest influence on the annual transparency of JZB. COVID-19 significantly reduced human activities, leading to the highest increase in transparency from 2019 to 2020. As the epidemic gradually stabilized from 2021 to 2022 and human activities resumed—including the disposal of medical waste—the rate of increase in transparency decreased. In 2022, transparency began to decrease, and the increase in annual rainfall more fully reflected the significant impact of human activities on the annual variation in JZB's transparency. Over the past decade, various policies enacted by the Qingdao Municipal Government have partially mitigated ecological damage and enhanced water transparency in JZB.

REFERENCES

[1] H. Ye, X. Liao, X. He, and H. Yue, "Remote sensing monitoring and variation analysis of marine ecological environment in coastal waters of Sri Lanka," *Geo-Inf. Sci.*, vol. 22, no. 7, pp. 1463–1475, 2020.

[2] L. Yang et al., "Remote sensing retrieval of Secchi disk depth in Jiaozhou Bay using Sentinel-2 MSI image," *Infrared Laser Eng.*, vol. 50, no. 12, 2021, Art. no. 20210080.

[3] Y. Zhou et al., "Variations of water transparency and impact factors in the Bohai and Yellow seas from satellite observations," *Remote Sens.*, vol. 13, no. 3, 2021, Art. no. 514.

[4] Y. Zhou et al., "Monitoring multi-temporal and spatial variations of water transparency in the Jiaozhou Bay using GOCI data," *Mar. Pollut. Bull.*, vol. 180, 2022, Art. no. 113815.

[5] B. Han et al., "Development of a semi-analytical algorithm for the retrieval of suspended particulate matter from remote sensing over clear to very turbid waters," *Remote Sens.*, vol. 8, no. 3, 2016, Art. no. 211.

[6] Y. Li, F. Wang, and X. Ren, "Development trend and strategy of ocean observing capability," *Adv. Earth Sci.*, vol. 25, no. 7, pp. 715–722, 2010.

[7] I. M. Suffian, S. H. Lee, A. R. Md, and S. M. Jafar, "Two-decade dynamics of MODIS-derived Secchi depth in Peninsula Malaysia waters," *J. Mar. Syst.*, vol. 236, 2022, Art. no. 103799.

[8] M. A. Daniel, J. Dalin, and M. Bunkei, "A semianalytical algorithm for estimating water transparency in different optical water types from MERIS data," *Remote Sens.*, vol. 14, no. 4, 2022, Art. no. 868.

[9] F. Yousef, R. Shuchman, M. Sayers, G. Fahnenstiel, and A. Henareh, "Water clarity of the upper great lakes: Tracking changes between 1998–2012," *J. Great Lakes Res.*, vol. 43, no. 2, pp. 239–247, 2016.

[10] Y. Zhou, D. Yu, X. Liu, Q. Yang, and Y. Gai, "Research on remote sensing retrieval and diurnal variation of Secchi disk depth of Jiaozhou Bay based on GOCI," *Remote Sens. Natural Resour.*, vol. 33, no. 2, pp. 108–115, 2021.

[11] C. Zhang and Y. Zeng, "Remote sensing monitoring and spatial-temporal change of seawater transparency in Taiwan Strait," *J. Meteorol. Environ.*, vol. 31, no. 2, pp. 73–81, 2015.

[12] H. Yao et al., "Spatiotemporal variation characteristics and driving factors of water transparency in the Yellow Sea from 2003 to 2020," *Mar. Environ. Sci.*, vol. 42, no. 2, pp. 262–270, 2023.

[13] Z. Lee et al., "Secchi disk depth: A new theory and mechanistic model for underwater visibility," *Remote Sens. Environ.*, vol. 169, pp. 139–149, 2015.

[14] Z. Lee, S. Shang, L. Qi, J. Yan, and G. Lin, "A semi-analytical scheme to estimate Secchi-disk depth from Landsat-8 measurements," *Remote Sens. Environ.*, vol. 177, pp. 101–106, 2016.

[15] L. Ma, X. Yang, Y. Qi, Y. Liu, and J. Zhang, "Oceanic area change and contributing factor of Jiaozhou Bay," *Scientia Geographica Sinica*, vol. 34, no. 3, pp. 365–369, 2014.

[16] W. Wang, "Natural environment of Jiaozhou Bay," *Coastal Eng.*, vol. 3, pp. 18–24, 1986.

[17] L. Gao, H. Yao, M. Zhang, L. Ju, and J. Cao, "Temporal and spatial variation of seawater transparency and its relationship with environmental factors in Qingdao coastal area," *J. Mar. Sci.*, vol. 35, no. 3, pp. 79–84, 2017.

[18] Y. He et al., "Water clarity mapping of global lakes using a novel hybrid deep-learning-based recurrent model with Landsat OLI images," *Water Res.*, vol. 215, 2022, Art. no. 118241.

[19] L. G. Olmanson, M. E. Bauer, and P. L. Brezonik, "A 20-year Landsat water clarity census of Minnesota's 10,000 lakes," *Remote Sens. Environ.*, vol. 112, no. 11, pp. 4086–4097, 2008.

[20] Z. Zheng, N. Sun, and Y. Li, "Analysis of hydrological changes in last 20 years in Dagu river basin of Qingdao," *Shandong Water Resour.*, no. 11, pp. 10–12, 2022.

[21] G. R. North, "Empirical orthogonal functions and normal modes," *J. Atmos. Sci.*, vol. 41, no. 5, pp. 879–887, 1984.

[22] F. Su, W. Wu, B. Ping, J. Yi, and Y. Zhang, "Research progress of the marine geographic information system," *Mar. Sci. Bull.*, vol. 33, no. 4, pp. 361–370, 2014.

[23] Z. Yin, T. Jiang, G. Yang, J. Huang, and Y. Zhao, "The spatial-temporal variation of water clarity and its influencing factors in Jiaozhou Bay from 1986 to 2017," *Mar. Sci.*, vol. 44, no. 4, pp. 21–32, 2020.

[24] Y. Chen, D. Song, X. Bao, and Y. Yan, "Impact of the cross-bay bridge on water exchange in Jiaozhou Bay, Qingdao, China," *Oceanologia et Limnologia Sinica*, vol. 50, no. 4, pp. 707–718, 2019.

[25] S. Han, J. Zhao, F. Wei, and J. Lin, "3D numerical simulation of the fresh water and sediment in the Dagu estuary of Jiaozhou Bay during the flood season," *Periodical Ocean Univ. China*, vol. 37, no. 5, pp. 689–694, 2007.

[26] H. Ye et al., "Assessment of water quality in the Eastern China seas based on water transparency satellite products," *Mar. Environ. Sci.*, vol. 42, no. 4, pp. 523–533, 2023.

[27] G. Camps-Valls et al., "A unified vegetation index for quantifying the terrestrial biosphere," *Sci. Adv.*, vol. 7, no. 9, 2021, Art. no. eabc7447.

[28] J. Gao, X. Mu, and W. Sun, "Temporal and spatial variations in vegetation cover on the loess plateau from 1981 to 2012," *Soil Water Conservation China*, no. 7, pp. 52–56, 2016.

[29] M. Kalina and E. Tilley, "'This is our next problem': Cleaning up from the COVID-19 response," *Waste Manage.*, vol. 108, pp. 202–205, 2020.

[30] Q. Jiang, Z. Xu, and H. Zhang, "Global impacts of COVID-19 on sustainable ocean development," *Innovation*, vol. 3, no. 4, 2022, Art. no. 100250.

[31] M. Wang, W. Zheng, and F. Li, "Application of Himawari-8 data to enteromorpha prolifera dynamically monitoring in the Yellow Sea," *J. Appl. Meteorol. Sci.*, vol. 28, no. 6, pp. 714–723, 2017.

[32] Y. Dong, Y. Liu, C. Hu, I. R. Macdonald, and Y. Lu, "Chronic oiling in global oceans," *Science*, vol. 376, no. 6599, pp. 1300–1304, 2022.

Dingfeng Yu (Member, IEEE) received the Ph.D. degree in environmental science from the Yantai Institute of Coastal Zone Research, Chinese Academy of Sciences, Yantai, China, in 2013.

He is currently an Associate Professor with the Institute of Oceanographic Instrumentation, Qilu University of Technology (Shandong Academy of Sciences), Qingdao, China. He has authored or coauthored some articles in the IEEE journal and IEEE conferences. His main research interests include ocean color remote sensing and signal processing.

Tengda Qi received the bachelor's degree in software engineering from the Hebei University of Economics and Business, Shijiazhuang, China, in 2016. He is currently working toward the master's degree in computer technology with the Qilu University of Technology, Qingdao, China.

His research interests include ocean remote sensing and the development of Java programs.

Lei Yang received the B.S. and M.S. degrees in communication engineering from the Harbin Institute of Technology, Harbin, China, in 2011 and 2013, respectively.

He is currently a Research Scientist with the Institute of Oceanographic Instrumentation, Qilu University of Technology (Shandong Academy of Sciences), Qingdao, China. His research interests include data analysis and processing, system design, remote sensing, and array signal processing.

Yan Zhou received the B.S. and M.S. degrees in marine information detection and processing from the Ocean University of China, Qingdao, China, in 2007 and 2011, respectively.

She is currently a Research Assistant with the Institute of Oceanographic Instrumentation, Qilu University of Technology (Shandong Academy of Sciences), Qingdao, China. Her research interests include remote sensing retrieval and application of ocean color, calibration verification of microwave scatterometers, and comprehensive analysis and processing of ocean remote sensing data.

Chunyan Zhao received the bachelor's degree in electrical engineering and automation from Qingdao Agricultural University, Qingdao, China, in 2020. She is currently working toward the master's degree in electronic information with the Qilu University of Technology (Shandong Academy of Sciences), Qingdao.

Her research interests include ocean remote sensing and data analysis.

Shunqi Pan received the Ph.D. degree in fluid mechanics from Heriot-Watt University, Edinburgh, U.K., in 1993.

He is currently a Professor of coastal engineering and the Director of Hydro-Environmental Research Centre, School of Engineering, Cardiff University, Cardiff, U.K. He has many years of research experience in coastal engineering, including physical and numerical modeling of coastal and estuarine processes. His recent interest is marine environmental monitoring.